Fractal pore distribution and magnetic microstructure of pulse-electrodeposited nanocrystalline Ni and Co

R. Przeniosło
Department of Physical Chemistry, University of Saarland, D-66123 Saarbrücken, Germany
and Institute of Experimental Physics, Warsaw University, Hoża 69, PL-00681, Warsaw, Poland

R. Winter,* H. Natter, M. Schmelzer, and R. Hempelmann†
Department of Physical Chemistry, University of Saarland, D-66123 Saarbrücken, Germany

W. Wagner
Paul Scherrer Institute, CH-5232 Villigen, Switzerland
(Received 26 April 2000; published 4 January 2001)

The crystalline and magnetic microstructures of nanocrystalline Ni and Co samples, with volume-averaged grain sizes between 10 and 60 nm, obtained by pulsed electrodeposition have been studied by means of small angle neutron scattering (SANS), small angle x-ray scattering (SAXS), and magnetization measurements. According to density measurements the porosity of the samples amounts to values between 0.5 and 3 %. SAXS and nuclear SANS contributions are dominated by pore scattering and reveal that the pores are distributed according to a fractal correlation function. The magnetic SANS contributions measured at zero field indicate that both *n*-Ni and *n*-Co have magnetic domains with sizes exceeding 150 nm, i.e., the domains must confine several crystallite grains. The present results of the domain sizes in *n*-Ni are similar to earlier literature data. For the case of *n*-Co the present results differ considerably from literature data, where only single-grain domains were found in *n*-Co samples synthesized by other methods. We attribute the difference in domain sizes in *n*-Co to the preparation method which in the present case yields samples of relatively high density. The field dependence of the SANS signal observed in *n*-Ni and *n*-Co shows that large domains are saturated at smaller fields than the smaller domains. The field dependence of the SANS signal is compared with the field dependence of the magnetization.

DOI: 10.1103/PhysRevB.63.054408 PACS number(s): 75.50.Kj, 61.46.+w, 61.12.Ex, 61.10.Eq

I. INTRODUCTION

Nanostructured materials, i.e., materials with grain sizes in the order of 5–100 nm can have properties which differ substantially from those of the corresponding polycrystalline materials. The main reason for this is the small grain size and the relatively high volume fraction of the grain boundary regions in which the atoms have to accommodate to the different alignment of neighboring grains. The morphology of these materials can influence their thermal properties, such as specific heat and thermal expansion coefficients, mechanical properties such as elastic moduli and hardness, as well as electronic properties such as resistivity. An extended review of the properties of nanocrystalline materials is given in Ref. 1.

In this paper we are concerned with the magnetic properties of nanocrystalline ferromagnetic metals Ni (*n*-Ni) and Co (*n*-Co). Conventional polycrystalline ferromagnetic materials have a domain structure, called magnetic microstructure, with sizes in the μm range. In nanostructured materials the grain size can be much smaller than the typical domain size, and it becomes comparable to the thickness of a domain wall. In addition the magnetic moments in grain boundary regions can be altered and thus influence the macroscopic magnetic properties of the material. It is known that in systems of consolidated nanoparticles the magnetic interactions can extend over several grains giving domains much larger than the single grain size as it was already shown for *n*-Fe (Ref. 2) and *n*-Ni (Refs. 3,4).

The basic question on the relationship between the crystalline microstructure and the magnetic microstructure of nanocrystalline metals has already been studied by small angle neutron scattering (SANS) and magnetization measurements by Löffler *et al.*[3–6] The samples used in these studies were synthesized by inert gas condensation (IGC) and ball milling (BM) (Refs. 7,8) and their densities were of the order of 80–90 % of the bulk material density. In this paper we deal with studies of *n*-Ni and *n*-Co samples prepared by the pulsed electrodeposition (PED) method which yields larger relative densities of the order of 95–98.5%. Because of the higher density of the samples obtained by PED we expect that the grain boundary regions can have a different morphology and the crystallites can occupy a larger part of the sample volume. Therefore we are interested whether this different crystalline microstructure can change the magnetic properties of the material.

We used experimental techniques which can provide information about the crystalline microstructure, i.e., small angle neutron scattering (SANS) and small angle x-ray scattering (SAXS).[9,10] The magnetic properties were studied by macroscopic magnetization measurements and by magnetic SANS.[9,11]

TABLE I. Parameters of the microstructure of *n*-Ni and *n*-Co. $2R$ is the volume averaged diameter of the grains obtained from Warren-Averbachs' method (Refs. 12,13,15) for *n*-Ni, and from the Scherrer formula for *n*-Co. D_{SANS} and D_{SAXS} refer to the volume fractal dimensions of SANS (nuclear contribution) and SAXS, respectively. ξ_{SANS} and ξ_{SAXS} refer to the fractal correlation lengths. ϕ denotes the volume fraction of pores obtained from the nuclear SANS contribution using Eq. (9). ρ_{rel} is the relative density determined by Archimedes' method. (n.m.) means not measured.

Sample	$2R$[nm]	D_{SANS}	D_{SAXS}	ξ_{SANS}[nm]	ξ_{SAXS}[nm]	ϕ[%]	ρ_{rel}[%]
Ni No. 7	20	2.84(1)	2.98(5)	26(2)	24(2)	0.09	98.4
Ni No. 17	25	2.79(4)	2.80(4)	85(30)	42(8)	0.11	97.0
Ni No. 13	57	2.81(2)	2.74(8)	63(12)	33(6)	0.15	95.3
Co No. 1	13	2.95(2)	2.88(2)	>200	>200	2.26	98.5
Co No. 3	15	2.90(5)	n.m.	>200	n.m.	1.05	98.4

II. MATERIALS AND METHODS

The *n*-Ni and *n*-Co samples were prepared by the PED technique.[12,13] The electrodeposition of *n*-Ni and *n*-Co was carried out using a Ni and Co sacrificial anode and an inert Ti cathode with dimensions 20 mm×20 mm. The electrolyte solution contained Na-K tartrate (120 g/l), boric acid (24 g/l), NH_4Cl (40 g/l), and Na saccharin (0–2 g/l). $NiSO_4$(40 g/l) and $CoSO_4$ (40 g/l) were used for *n*-Ni and *n*-Co deposition, respectively. The modulated currents were generated by a signal generator which controlled a bipolar operation source combined with a galvanostatic unit in order to keep the current at constant value during the pulse. The bath temperature was kept constant during each electrodeposition, and the temperature values varied between 25 and 55 °C. The current was applied in rectangular pulses of duration t_{on} between 1–5 ms interrupted by t_{off} periods between 50 and 100 ms. The resulting nanocrystalline deposits were mechanically removed from the cathode by a sharp knife thus forming thin foils.

The crystalline microstructure was first characterized by wide angle x-ray diffraction using a Siemens D500 x-ray diffractometer with incident Cu$K_{\alpha_{1/2}}$ radiation and a graphite analyzer crystal between the sample and the detector. The x-ray diffraction patterns of the *n*-Ni samples contained only broad diffraction peaks due to the crystalline fcc structure.[14] The diffractograms of *n*-Ni have been analyzed using the Warren-Averbach method[15] implemented in a computer program FALTER,[18] and the volume averaged diameters of the nanocrystalline grains have been estimated (see Table I). The grain size distribution is best described by the log-normal distribution function introduced in Ref. 16:

$$g(D)=\frac{1}{\sqrt{2\pi}D\ln\sigma}\exp\left[-\frac{1}{2}\left(\frac{\ln(D/D_0)}{\ln\sigma}\right)^2\right], \qquad (1)$$

where D is the grain diameter, D_0 is the median diameter, and σ is the variance of the distribution. For our *n*-Ni samples σ amounts to values between 1.2 and 1.4. The x-ray data obtained from the *n*-Co samples show much worse statistics because x-ray Cu$K_{\alpha_{1/2}}$ radiation corresponds to an energy which is close to the absorption edge of Co, therefore we observe a higher background and smaller count rates than in the *n*-Ni case. The x-ray diffractograms of *n*-Co show broad reflections due to the hexagonal phase of Co.[17] The grain size of the nanocrystalline grains of Co was estimated according to the Scherrer formula.[11]

The resulting samples were thin foils of a surface area close to the electrode square size, i.e., 20 mm×20 mm, and of a thickness varying from 10 to 50 μm. The densities of the samples have been measured using Archimedes's method. The mass of the samples was measured in air and in liquid diethylphtalate (density 1.1175 g/cm^3) using a Mettler MT5 FACT balance. The obtained values of density are of the order of 97.0–98.5 % of the bulk Ni and Co density (see Table I). The oxygen content of some selected *n*-Ni and *n*-Co samples was determined by hot extraction in a helium gas flow combined with infrared spectroscopy. The resulting oxygen contents varied from 0.03 to 0.30 wt. %. The metal impurity contents in another set of *n*-Ni samples obtained from the PED method have been reported[12] to be small, i.e., of the order of 100–1000 ppm.

The SANS measurements have been performed at the small angle neutron scattering instrument (SANS) at SINQ (Villigen, Switzerland) using a neutron wavelength $\lambda = 0.6$ nm and three sample-detector distances of 1.8, 6, and 20 m. The Q-range covered was $0.04\,\mathrm{nm}^{-1} \leqslant Q \leqslant 3.40\,\mathrm{nm}^{-1}$, where the modulus of the scattering vector is defined as $Q=(4\pi/\lambda)\sin\Theta$, with the scattering angle being 2Θ. The thin foil samples were placed between the poles of an electromagnet which could provide a dc horizontal magnetic field parallel to the sample surface and thus perpendicular to the incident beam. The SAXS measurements were performed using a pinhole camera[18] equipped with a rotating Cu anode and a Si(111) single crystal monochromator. The measurements were done with a sample-detector distance of 3 m giving a Q range of $0.03\,\mathrm{nm}^{-1} < Q < 0.5\,\mathrm{nm}^{-1}$. This Q range contains the desired information; therefore shorter detector distances have not been used. The magnetization measurements were performed at room temperature with an EG&G PARC Model 458A vibrating sample magnetometer at the Laboratory for Technical Physics, University of Saarbrücken.

III. SMALL ANGLE SCATTERING

Small angle scattering (SAS) is a well-established technique suitable for studies of the microstructure in the nanometer length range of solids. SAXS measurements yield information about the crystalline microstructure[10] while in

SANS measurements we observe both nuclear and magnetic scattering contributions.[9] For Ni and Co samples the nuclear coherent scattering lengths are $b_{\mathrm{coh}}(Ni)=10.3\times10^{-15}$ m and $b_{\mathrm{coh}}(\mathrm{Co})=2.49\times10^{-15}$ m[19] and the corresponding magnetic coherent scattering lengths are equal to $b_{\mathrm{mag}}=2.7M$, where M is the value of the fully saturated magnetic moments given in μ_B.[11] For the case of Ni we obtain $b_{\mathrm{mag}}=1.67\times10^{-15}$ m and for Co $b_{\mathrm{mag}}=4.63\times10^{-15}$ m.[20] To compare the size of the magnetic and nuclear contributions we calculate the squared ratio of the magnetic to nuclear coherent neutron scattering lengths[11] $(b_{\mathrm{mag}}/b_{\mathrm{coh}})^2$. For Ni it is equal to 0.025, i.e., it is much smaller than for Co where it is 3.457. In the following discussion we will use the scattering length density ρ defined as $\rho=b/V$ where b is the scattering length of one atom and V is the average volume occupied by one atom.

In order to obtain the SANS differential scattering cross section $d\Sigma/d\Omega(Q)$ in absolute units of $\mathrm{cm}^{-1}\,\mathrm{sr}^{-1}$ the scattered intensity has to be corrected and normalized to the incoherent scattering of a standard sample, which is usually water.[21] In the case of SAXS we used the cross sections in relative units. The two-dimensional SANS signal measured at the sample in a saturating magnetic field should be composed of an isotropic nuclear contribution and an anisotropic magnetic contribution. In such a case the magnetic moments **M** are all parallel to the external field $\mathbf{B}_0$ and the nuclear and magnetic cross sections can be separated from each other by fitting the two-dimensional SANS signal to the following formula:[9]

$$d\Sigma/d\Omega=d\Sigma/d\Omega_{\mathrm{nuc}}(Q)+d\Sigma/d\Omega_{\mathrm{mag}}(Q)\sin^2\alpha, \qquad (2)$$

where α is the angle between the scattering vector **Q** and the magnetization **M** in the plane of the detector and $\alpha=0$ for **Q** parallel to **M**. For further data evaluation the nuclear and magnetic contributions of the two-dimensional SANS signal were averaged with regard to the azimuthal angle α in the detector plane, giving the radial scattering cross sections for nuclear $d\Sigma/d\Omega_{\mathrm{nuc}}(Q)$ and magnetic $d\Sigma/d\Omega_{\mathrm{mag}}(Q)$ scattering, respectively. In the case of SANS measurements in zero field or SAXS measurements the observed signal should be isotropic and the angular averaging has also to be performed. If the sample consists of single grain domains in which all the atoms have the same values of the magnetic moments, then the nuclear and magnetic SANS contributions are both proportional to the same structure function $F(Q)$. In such a case the angular averaging of the cross section given in Eq. (2) gives for saturated magnetic moments[4,9]

$$\frac{d\Sigma}{d\Omega}(Q)=\left(b_{\mathrm{nuc}}^2+\frac{1}{2}b_{\mathrm{mag}}^2\right)F(Q) \qquad (3)$$

and for randomly oriented domains

$$\frac{d\Sigma}{d\Omega}(Q)=\left(b_{\mathrm{nuc}}^2+\frac{2}{3}b_{\mathrm{mag}}^2\right)F(Q). \qquad (4)$$

A model independent evaluation of the SANS data can be performed using the so-called Porod invariant[9] $\tilde{Q}$. It is assumed that the system is composed of scatterers occupying a volume fraction ϕ and a uniform matrix occupying the rest of the volume, i.e., $(1-\phi)$. The difference between the scattering length densities between these two types of matter equals $\Delta\rho$. It is possible to estimate the volume fraction ϕ without any knowledge of the internal structure of the material. Provided the scattering cross section is known in absolute units one has to perform the following integration:[9]

$$\tilde{Q}=\int_0^\infty Q^2\frac{d\Sigma}{d\Omega}(Q)dQ=2\pi^2\phi(1-\phi)(\Delta\rho)^2. \qquad (5)$$

For a system composed of scattering objects with well-defined smooth surfaces the asymptotic part of the small angle scattering cross section should obey the Porod law[10]

$$d\Sigma/d\Omega(Q)\propto Q^{-4}. \qquad (6)$$

The Porod law is not always fulfilled and there are several SAS studies where a $Q^{-\alpha}$ behavior with $\alpha<4$ was found. These effects can be explained in terms of a fractal microstructure.[22,23] *Surface* fractals with fractal dimensions $2\leqslant D_S\leqslant3$ contributing to SAS with exponents $3\leqslant\alpha=6-D_S\leqslant4$ were found in studies of lignite coal[24] and sandstones[25] whereas *volume* fractals with fractal dimensions $2\leqslant D\leqslant3$ giving exponents $2\leqslant\alpha=D\leqslant3$ were found in silica aerogels.[26,27] Exponents between 3 and 4 were also reported in SAXS studies of IGC *n*-Pd (Ref. 28) and SANS studies of Al/Al_2O_3.[29]

We assume that our material contains empty pores which are not randomly distributed, but that their distribution fulfills the definition of volume fractals, i.e., within a sphere of radius R the average number of objects is proportional to R^D, where D is the volume fractal dimension.[22] In such a case the correlation function has the form[27] $\gamma(R)=AR^{D-3}$, but according to the argument that fractal correlations cannot extend to infinity[27] we use a modified correlation function

$$\gamma(R)=AR^{D-3}\exp(-R/\xi), \qquad (7)$$

where ξ is the characteristic correlation length. We assume that the system is composed of bulk metal with constant scattering length density ρ and open pores with zero density (i.e., the density contrast $\Delta\rho=\rho$) occupying a fraction of the volume ϕ, and distributed according to a pair correlation function given in Eq. (7). The SANS cross section for this case is given by the following integral:[23]

$$\frac{d\Sigma}{d\Omega}=V(\Delta\rho)^2\phi(1-\phi)\int_0^\infty 4\pi R^2\gamma(R)\frac{\sin(QR)}{QR}dR. \qquad (8)$$

For the specific form of the pair correlation function given by Eq. (7) this yields[23]

$$\frac{d\Sigma}{d\Omega}=\frac{A(1+Q^2\xi^2)^{(1-D)/2}\sin[(D-1)\arctan(Q\xi)]}{Q\xi(D-1)}. \qquad (9)$$

IV. CRYSTALLINE MICROSTRUCTURE

A. SAXS and SANS results

In this section we analyze the SANS measurements performed in strong magnetic fields, i.e., 0.7 T for *n*-Ni and 1.0

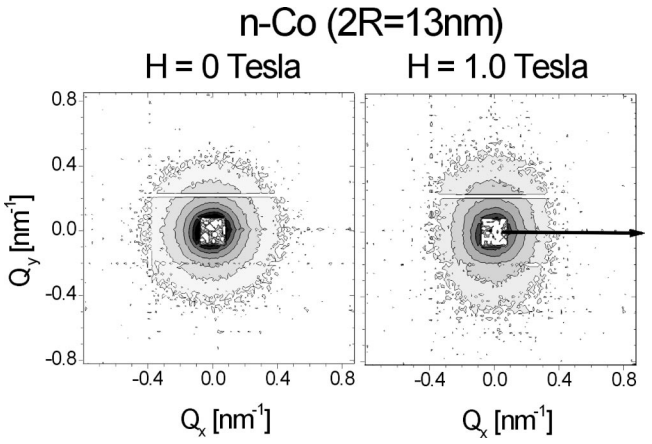

FIG. 1. Lines of equal SANS intensity on a two-dimensional position sensitive detector measured for *n*-Co with average grain size of $2R=13$ nm at zero field (left) and in a strong magnetic field of 1.0 T (right). The horizontal arrow denotes the external field direction.

T for *n*-Co. From magnetization studies of single crystals of Ni and Co (Ref. 20) as well as *n*-Ni (Ref. 5) and *n*-Co (Ref. 30) it is known that at such high fields essentially all the magnetic moments are aligned parallel to the field direction.

In the case of *n*-Ni the contribution of magnetic scattering is expected to be small and we actually did not observe any anisotropy of the SANS signal even at the maximum field of 0.7 T; thus we assume that all the observed signal is due to nuclear scattering. For further data evaluation the SANS signal of *n*-Ni was averaged with regard to the azimuthal angle α in the detector plane giving a radial scattering cross section. The two-dimensional SANS signal of *n*-Co measured in zero field and at 1.0 T is given in Fig. 1. One can see that it is elongated in a direction perpendicular to the external field direction B_0. The nuclear and magnetic contributions were separated from each other by fitting the anisotropic SANS signal with Eq. (2). The data reduction was carried out with the software package BERSANS.[31]

The nuclear SANS cross sections of all the studied *n*-Ni and *n*-Co samples show a non-Porod behavior, i.e., at large Q it is proportional to $Q^{-\alpha}$, with α between 2.8 and 3.0. Since we know that the density of the *n*-Ni and *n*-Co samples is of the order of 97–99 % of the bulk Ni and Co density, we can assume that the observed SANS is due to empty pores which should occupy around 1–3 % of the sample volume. The cross section given by Eq. (9) with an additional constant background value was fitted to the radial nuclear scattering cross sections of SANS and radial SAXS cross sections. The results of a representative fit for one *n*-Ni sample is shown in Fig. 2, and the resulting fit parameters for all samples are shown in Table I. One can see from Fig. 2 that the model gives a satisfactory fit to the experimental data. Both the SANS and SAXS signals tend to a saturation at low Q, and the fractal correlation length ξ is of the order of the grain size.

The results of a representative fit for one *n*-Co sample is shown in Fig. 3 where both SANS and SAXS signals do not saturate at low Q. For $\xi > 200$ nm the cross section given by

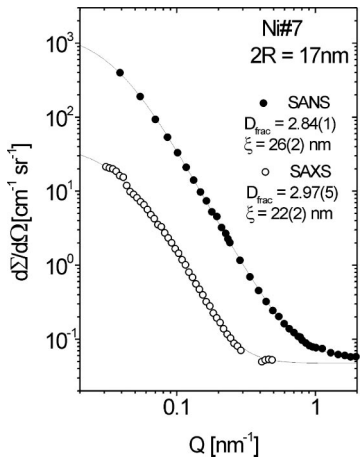

FIG. 2. Radial nuclear SANS cross section given in absolute units (solid circles) and SAXS cross section given in arbitrary units (open circles) measured on the same sample of *n*-Ni with volume averaged grain diameter $2R=17$ nm, shown as a function of the modulus of the scattering function (see text). Due to a relatively small value of the fractal correlation length ξ, one can see a saturation of the function at low Q.

Eq. (8) is proportional to Q^{-D} in the whole measured Q range; therefore, for the scattering curves which did not show any saturation at low Q, a constant value of $\xi=200$ nm was kept fixed during the fit. In the studies of aerogels[27] it was assumed that at the largest Q values the scattering function is dominated by the single particle form factor yielding a Porod law behavior and the scattering function used was slightly different from Eq. (9). In our treatment of *n*-Ni and *n*-Co we do not assume any specific shape of the pores, but we assume that they are small (i.e., of the order of 1–2 nm), so their shape might only influence the large Q limits of the measured SANS and SAXS signals, which in our measurements are dominated by the background.

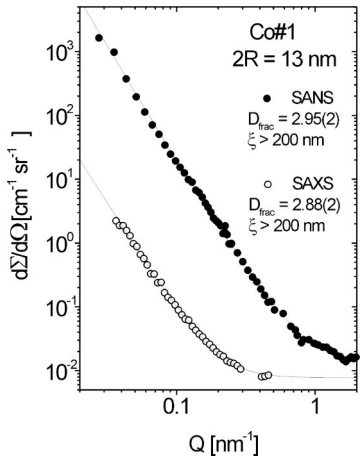

FIG. 3. Radial nuclear SANS cross section given in absolute units (solid circles) and SAXS cross section given in arbitrary units (open circles) measured on the same sample of *n*-Co with volume averaged grain diameter $2R=13$ nm, shown as a function of the modulus of the scattering vector Q. The continuous line is a result of the fit made with a volume fractal scattering function (see text).

In order to check if this assumption is correct and the scattering can be due to empty pores we have calculated the Porod invariant [Eq. (5)] by using the function $(d\Sigma/d\Omega)$ resulting from the best fit to SANS data [Eq. (9)]. Taking into account the molar densities and coherent scattering lengths of Ni and Co the scattering length density contrasts used are $\Delta\rho_{\mathrm{Ni}}=9.408\times10^{10}\,\mathrm{cm}^{-2}$ and $\Delta\rho_{\mathrm{Co}}=2.254\times10^{10}\,\mathrm{cm}^{-2}$, and the calculated volume fractions of scatterers ϕ are shown in Table I. In the calculation of the integral in Eq. (5) one has to extrapolate to Q values outside the measurement range and we used $Q=10\,\mathrm{nm}^{-1}$ as the upper limit for integration. This corresponds to the size of a single atom.

B. Discussion of crystalline microstructure

Nanocrystalline solids consist of nanometer sized crystalline grains embedded in grain boundary regions. The small size of the crystallites gives rise to a broadening of the x-ray diffraction peaks which we observed in all our *n*-Ni and *n*-Co samples. Earlier SANS studies of *n*-Ni and *n*-Co obtained by IGC or BM (Refs. 6,32) found that the grain boundary regions have a reduced density compared to the density of the crystallites. The nuclear SANS contributions of IGC *n*-Ni and *n*-Co were quantitatively interpreted as scattering from spherical crystallite grains, and the average grain sizes obtained from SANS and x-ray diffraction were similar.[4] According to our present SANS and SAXS studies of PED *n*-Ni and *n*-Co we can say that the grain boundary density is similar to the density of the crystallites. From density measurements we obtain values between 97 and 99 % of the bulk metal density what would correspond to porosities from 3 to 1 %. From a model independent Porod invariant we calculate the volume fraction of empty pores ϕ and obtain about 1 to 2 % in *n*-Co (see Table I). In the case of *n*-Co pores are definitely the dominant scatterers because the Porod invariant estimations and macroscopic density measurements agree with each other. For *n*-Ni, ϕ is of the order of 0.1%. The discrepancy between Porod invariant estimations and density measurements could be explained in the following way. The grain boundary morphology of fcc *n*-Ni can be different from that of hcp *n*-Co. It means that in the grain boundary regions where the atoms have to accommodate to the different orientations of the grains there may be a relatively large number of voids (i.e., missing single atoms) which have too small a size to contribute to the observed SANS. On the other hand there could be also pores larger than 150 nm which are too large to be detected by the SANS measurements.

It is important to note that the fractal dimensions observed in our studies are near to $D=3$ and that within experimental accuracy they are all smaller than 3 so the volume fractal model gives the best description. The nontrivial limit when the volume fractal dimension D and the surface fractal dimensions D_S tend to the value of 3 was discussed in Ref. 23. This corresponds to the case of a porous solid that is sufficiently compacted in such a way that both the volume and the internal surface become uniformly space filling. In the analysis of the SAS data we did not make any specific statement about the pore size nor the pore shape but only about the correlation between the positions of the pores given by Eq. (7). The pores are supposed to be the so-called triple junction voids which are located in corners where grain boundaries of several grains meet together. If we assume that during the process of pulsed electrochemical deposition there is a preference for smaller grains to cluster together, and that such clusters of smaller grains are surrounded by larger grains, then the distribution of the positions of triple junction voids could be described by a function such as that from Eq. (7), i.e., more pores are found near the cluster center and less further away from the center. An example of such a self-similar fractal microstructure observed in a SEM micrograph of one of our *n*-Ni samples is shown in Fig. 4. If the crystallite grains form a self-similar structure then the triple junctions have fractally correlated positions.

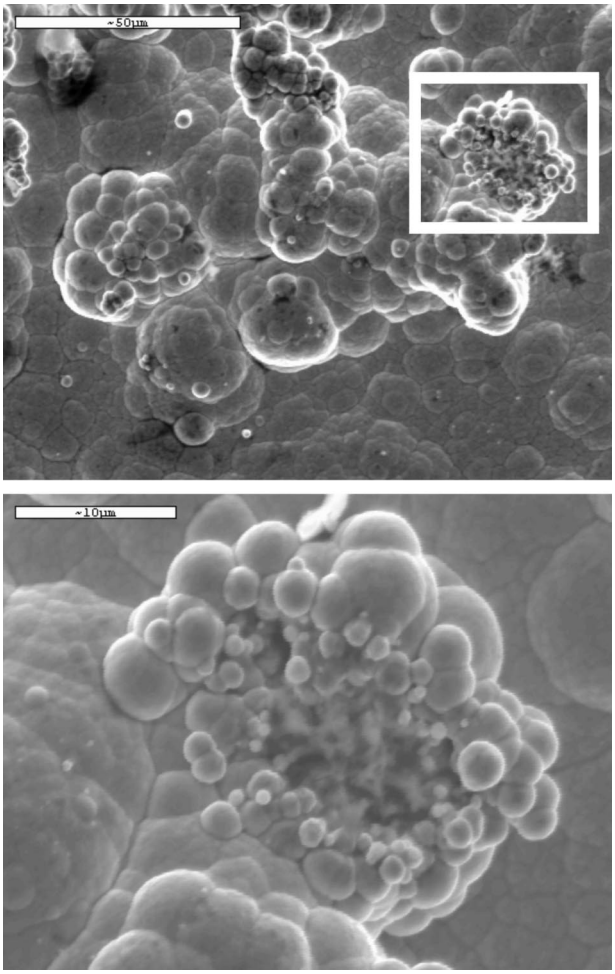

FIG. 4. SEM micrograph of the *n*-Ni sample with average grain size of 17 nm. The area marked with the black frame on the top picture is enlarged on the bottom picture. One can see the self-similar morphology of the crystallites.

We emphasize that the fractal pore distribution is a specific property of PED *n*-Ni and *n*-Co. Earlier SANS studies of *n*-Co and *n*-Ni obtained by IGC (Refs. 2–4,33) and ball milling[4] did not detect deviations from Porod's law.

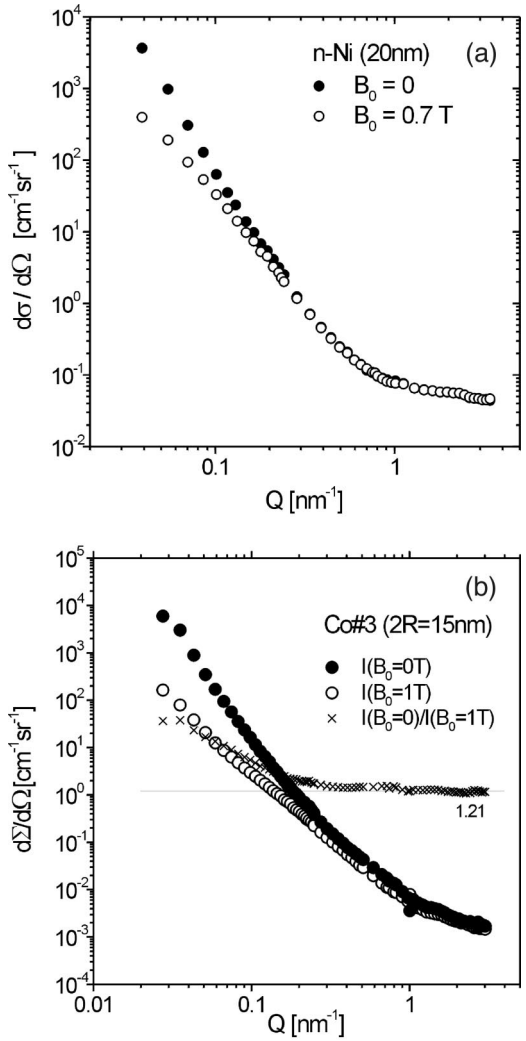

FIG. 5. (a) Radial SANS cross section measured on a *n*-Ni sample with grain size 20 nm measured in zero field (closed circles) and maximal external field of 0.7 T (open circles). (b) Radial SANS cross section measured on a *n*-Co sample with grain size 15 nm measured in zero field (closed circles) and maximal external field of 1.0 T (open circles). The ratio between the intensity of the SANS contribution measured in zero field to the contribution at $B_0=1$ T is marked by crosses.

V. MAGNETIC PROPERTIES

A. Magnetic microstructure at zero and high fields

Figures 5(a) and 5(b) show the radially averaged cross section [as represented by Eqs. (3) and (4)] measured for a *n*-Ni sample with an average grain diameter of 20 nm [Fig. 5(a)] and a *n*-Co sample with average grain diameter of 15 nm [Fig. 5(b)] measured at zero and maximal external magnetic field. One can see that at large values of Q both scattering curves are equal for *n*-Ni [Fig. 5(a)] and they are parallel for *n*-Co [Fig. 5(b)]. At lower Q, the scattering cross section measured without field is about one order of magnitude larger. These results agree with earlier studies of *n*-Ni, *n*-Co, and *n*-Fe obtained by IGC.[3,4,33] We can assume that, when a strong external field is applied, the magnetic moments are forced to an alignment which extends to very large distances, beyond the resolution of the SANS experiment (i.e., they scatter to $Q<0.04\,\mathrm{nm}^{-1}$). The measurements in zero field show a significant contribution due to magnetic scattering at low Q which corresponds to domains with sizes much larger than the average diameter of the grains. One can assume that in zero field there are regions where the magnetic moments of the individual grains are correlated and that the size of these regions is larger than 150 nm. In the case of *n*-Ni this result is in agreement with earlier studies[3,4,33] in which magnetic correlation lengths above 150 nm were reported in IGC *n*-Ni. There is, however, one important difference between the results of this paper and earlier studies of Löffler *et al.*;[3] here the splitting between the scattering curves measured in zero-field and maximal field becomes observable at $Q=0.25\,\mathrm{nm}^{-1}$ (see Fig. 5), whereas for a sample of *n*-Ni obtained by IGC and with similar grain size this splitting occurred only below[3] 0.1 nm^{-1}. This difference between the SANS contributions at larger Q values means that in PED *n*-Ni the smallest domains are smaller than the smallest domains in IGC *n*-Ni. It should be mentioned here that a SANS study of *n*-Ni obtained by the PED method has recently been published by Michels *et al.*[34] These authors performed SANS on a *n*-Ni sample with average grain size of 18 nm in external magnetic fields from 0.2 to 1.8 T. Similar to our present results (see Fig. 5), they observed that for $Q<0.3\,\mathrm{nm}^{-1}$ the SANS signal decreases with increasing fields. The SANS signal they measured at the high field of 1.8 T shows also a non-Porod behavior. The interpretation of their SANS data is based on the theory of micromagnetics[35] and concerns the field dependence of the SANS signal at fixed values of Q without considering the functional Q dependence of the SANS signal. The authors of Ref. 34 treat the nuclear SANS contribution as a residual scattering and they do not discuss the crystalline microstructure of PED *n*-Ni.

In the case of *n*-Co (see Fig. 5), as in the case of *n*-Ni, we also do not observe any saturation of the low Q part of the SANS signal measured at zero field. We can therefore assume that the magnetic domains in *n*-Co are also larger than 150 nm. In the larger Q part (Fig. 5) the SANS signals measured with and without field are parallel on a double logarithmic plot. The ratio of the two SANS signals is marked in Fig. 5 by crosses and one can see that for $Q\geqslant 0.5\,\mathrm{nm}^{-1}$ this ratio is constant. According to Eqs. (3) and (4) the radially averaged SANS contribution for the case of randomly oriented magnetic moments ($B_0=0$) is proportional to $[(b_{\mathrm{nuc}})^2+(2/3)(b_{\mathrm{mag}})^2]$ whereas for saturated magnetic moments ($B_0=1$ T) it is proportional to $[(b_{\mathrm{nuc}})^2+(1/2)(b_{\mathrm{mag}})^2]$. If we insert the values of b_{nuc} and b_{mag} of Co given in Sec. III we obtain a ratio of 1.21 which agrees well with the experimental data. This result means that for $Q\geqslant 0.5\,\mathrm{nm}^{-1}$ and the corresponding size in real space, both the magnetic and nuclear SANS signal are due to the same structure factor $F(Q)$ and that the magnetic scattering is also due to empty pores embedded in a matrix of fully saturated ($B_0=1$ T) or randomly oriented ($B_0=0$ T) magnetic moments.

In order to study the contribution of the magnetic correlations at $B_0=0$ without nuclear contributions the radial SANS cross section measured at B_{max} was subtracted from

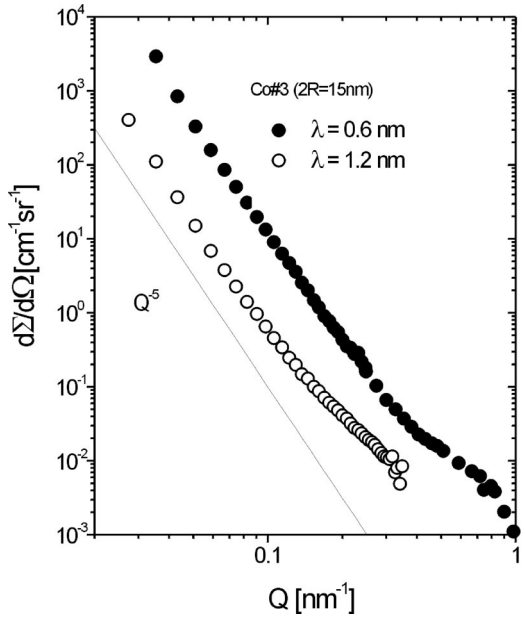

FIG. 6. Difference between the radial SANS cross section measured without field and with a maximal external magnetic field of 1.0 T for a *n*-Co sample with average grain size of 15 nm (wavelength 0.6 nm, solid circles). The empty circles represent the radial SANS cross section measured for the same sample without field with a wavelength of 1.2 nm. The straight line corresponds to a Q^{-5} power law.

the zero field SANS cross section. In the case of *n*-Ni the difference curve shows a power law behavior predicted by the Porod law, i.e., Q^{-4} in the accessible Q range, and there was no observable saturation at low Q. In the case of *n*-Co the difference curve shows, for $Q<0.5\,\mathrm{nm}^{-1}$, a power law behavior $Q^{-\alpha}$ with $4.6\leqslant\alpha\leqslant5.3$ and no saturation at low Q. A representative plot is shown in Fig. 6.

When the measured SANS cross sections show exponents larger than 4, one has to verify that this effect is not due to multiple scattering or multiple refraction of neutrons. Multiple scattering can be excluded here because of the small sample thickness ($t<40\,\mu$m). A possibility of multiple refraction[9] on several domains has also been considered. The index of refraction for neutrons with polarization vector parallel or antiparallel to the magnetization depends on the neutron wavelength. The SANS measurements for selected *n*-Ni and *n*-Co samples were repeated at a wavelength of 1.2 nm and the results did not show significant differences compared with the results obtained with $\lambda=0.6\,\mathrm{nm}$; hence we can conclude that there was no multiple refraction.

We can conclude that the magnetic correlations in *n*-Co at $B_0=0$ extend to sizes larger than the limitation of the SANS instrument, i.e., 150 nm. The exponent α larger than 4 can be due to scattering on magnetically ordered regions with nonsharp boundaries. As it was shown by Schmidt,[36] in a solid containing pores with a constant scattering length density ρ_0 and with boundaries where the density changes continuously for $0\leqslant x\leqslant a$, for instance, as $\rho(x)=\rho_0(x/a)^{\beta}$ (with $0\leqslant\beta\leqslant1$), the SANS intensity at large Q is proportional to $Q^{-\alpha}$ where $\alpha=4+2\beta$, i.e., $4<\alpha<6$. The case of magnetic ordering is much more complex because the magnetic moments at pore boundaries can have orientations different from those in the bulk material, but anyway the experimental data can be described in terms of this oversimplified model. It should be added that muon spin rotation (μSR) measurements performed on *n*-Ni and *n*-Co give an indication that the magnetically ordered regions might be surrounded by shells with magnetic disorder.[37] Similar conclusions were also drawn from perturbed γ-γ angular correlation spectroscopy (PAC) studies of PED *n*-Ni doped with a radioactive ^{111}In isotope.[38] These measurements have shown that in a *n*-Ni sample with 40 nm grain size a fraction of 37% of the atoms are located in a perturbed local magnetic environment which is different to the one observed in coarse-grained bulk polycrystalline Ni.

TABLE II. Values of the saturation magnetization measured for *n*-Ni and *n*-Co. The reference values come from measurements performed on a polycrystalline Ni and Co sample.

Sample	Grain size [nm]	Saturation magnetization [kA/m]
Ni	13	461
Ni	20	467
Ni	31	477
Ni	42	485
Ni	77	488
Ni	reference	491
Co	8	1387
Co	20	1423
Co	40	1429
Co	73	1421
Co	reference	1432

B. Magnetization measurements

We performed magnetization measurements and investigated the hysteresis loops of *n*-Ni with grain sizes between 13 and 77 nm and of *n*-Co with grain sizes from 8 to 73 nm, as well as a reference polycrystalline sample for both these metals.[30] The shape of the hysteresis loop changes in dependence on the grain size. With decreasing grain size, steeper hysteresis loops are observed and therefore, for smaller grains, the saturation magnetization could be reached at smaller external fields. The values of the saturation magnetization are given in Table II. In the case of *n*-Ni with small grain sizes we observed a slight reduction of the saturation magnetization by about 6% with respect to the reference polycrystalline Ni sample. A similar effect was observed in the case of *n*-Co.

For the case of *n*-Ni similar results were already reported in earlier studies of IGC *n*-Ni,[5,39] BM *n*-Ni,[40] and PED *n*-Ni,[41] where a slight reduction of the saturation magnetization was reported. Theoretical calculations performed for the case of *n*-Ni and *n*-Co show that the average magnetic moment in the grain boundaries is nearly the same as in the bulk[42] so one should not expect a strong dependence of the saturation magnetization on the grain size.

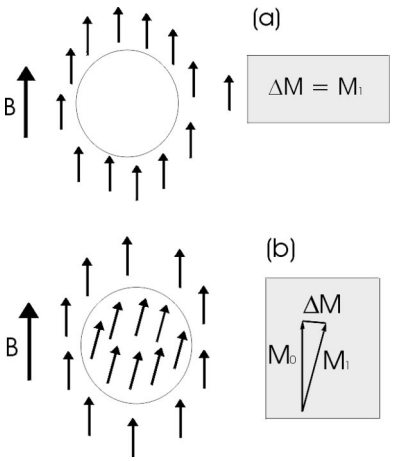

FIG. 7. (a) Schematic plot of an empty pore embedded in a uniformly magnetized matrix. Here the magnetization contrast $\Delta\mathbf{M}$ is parallel to the external magnetic field $\mathbf{B}_0$. (b) Schematic plot of a uniformly magnetized grain in a uniformly magnetized matrix. The magnetization directions of the grain $\mathbf{M}_1$ and the matrix $\mathbf{M}_0$ are slightly tilted with respect to each other. In this situation the magnetization contrast $\Delta\mathbf{M}$ is nearly perpendicular to the external field $\mathbf{B}_0$.

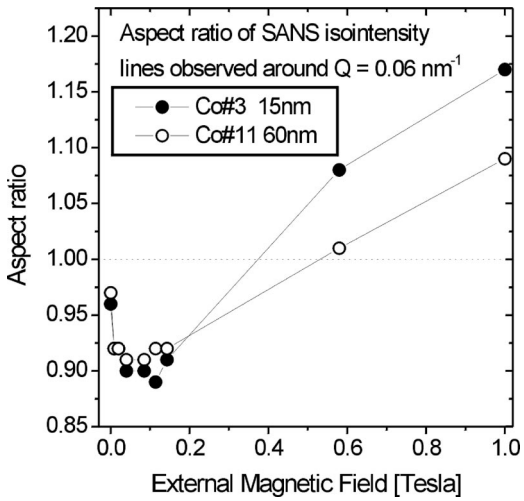

FIG. 8. Aspect ratio of the vertical (i.e., perpendicular to $\mathbf{B}_0$) to the horizontal axis of the SANS isointensity lines near $Q = 0.06\,\mathrm{nm}^{-1}$ obtained for n-Co samples with different grain sizes. The value of the aspect ratio is not equal to one at zero field (nearly isotropic SANS pattern) because the samples had a weak remanent magnetization.

C. Changes of the magnetic microstructure as a function of the field

The two-dimensional SANS signal observed for n-Co was isotropic at zero field and elongated in a direction perpendicular to $\mathbf{B}_0$ at the maximum field value of 1.0 T (see Fig. 1). The elongation perpendicular to the external field is expected at high field since the magnetization density contrast $\Delta\mathbf{M}$ is in high fields parallel to the field [see Fig. 7(a)] and the magnetic neutron scattering occurs only when Q is not parallel to $\Delta\mathbf{M}$.[9] Following the argumentation of Ref. 4 we have analyzed the aspect ratio of the constant intensity isolines of the two-dimensional SANS signal for different fields. The aspect ratio is the proportion of the lengths of the vertical and horizontal axis of the isointensity line as defined by Löffler *et al.*,[3] i.e., for an elongation perpendicular to the field the aspect ratio is larger than 1, and smaller than 1 for a parallel elongation. The aspect ratios for two n-Co samples with grain sizes of 15 and 60 nm are shown in Fig. 8. It is interesting to note that at intermediate fields, i.e., below 0.4 T, both n-Co samples have an aspect ratio smaller than unity. A similar behavior was already reported for IGC samples of n-Fe (Refs. 3,4) and n-Co in Ref. 4, where this effect was quantitatively explained. Following the interpretation given by Löffler[4] we can assume that the sample is a matrix with magnetic moments all parallel to $\mathbf{B}_0$ in which there are large ferromagnetic domains with magnetic moments tilted with respect to the direction of $\mathbf{B}_0$. This situation has been shown schematically in Fig. 7(b). In such a case the magnetic density contrast is a vector with its largest component perpendicular to $\mathbf{B}_0$, and the magnetic scattering occurs mostly in a direction parallel to $\mathbf{B}_0$. As will be shown later, in a field of 0.4 T the magnetization measurements yield a relative magnetization of at least 0.8. At the maximum field of 1 T the aspect ratios for the n-Co samples (see Fig. 8) are 1.10 and 1.14 what is much less than in the case of IGC n-Co samples for which a value of 1.30 was reported.[14,43] Such a large difference between the aspect ratios observed at the same external field means that in PED n-Co samples the SANS signal is less anisotropic and that their magnetic moments are less saturated than in ICG n-Co. This effect can be due to an incomplete alignment of domains in n-Co even at a field as large as 1.0 T.

For both n-Ni and n-Co the radial SANS signal changes gradually with increasing field. Our motivation was to find a trend in the field dependence of magnetic correlations by observing the changes of the SANS signal at several values of Q. Following the argumentation of Ref. 4 we considered the reduced SANS intensity $R(B_0,Q)$ defined as

$$R(B_0,Q)=\frac{I(0,Q)-I(B_0,Q)}{I(0,Q)-I(B_{\max},Q)}, \tag{10}$$

where $I(B_0,Q)$ represents the radial SANS cross section $d\Sigma/d\Omega(Q)$ measured at the external field B_0. The definition, Eq. (10), implies that $R(0,Q)=0$ and $R(B_{\max},Q)=1$; thus we expect that the field dependence of $R(B_0,Q)$ at fixed Q values should be similar to that of the reduced macroscopic magnetization. Indeed the similarity between the field dependence of $R(B_0,Q)$ and the reduced magnetization was already reported for n-Fe.[4] The relative magnetization measured with a magnetometer for a n-Ni sample with a grain size of 31 nm was compared with a reduced SANS intensity obtained for a n-Ni sample with a grain size of 25 nm. The results of both measurements are shown in Fig. 9. One can see that for low Q values, $R(B_0,Q)$ increases faster with increasing external field than for larger Q values. $R(B_0,Q)$ for the smallest measured $Q=0.039\,\mathrm{nm}^{-1}$ becomes saturated faster than the reduced macroscopic magnetization whereas the opposite behavior is observed for larger Q values such as

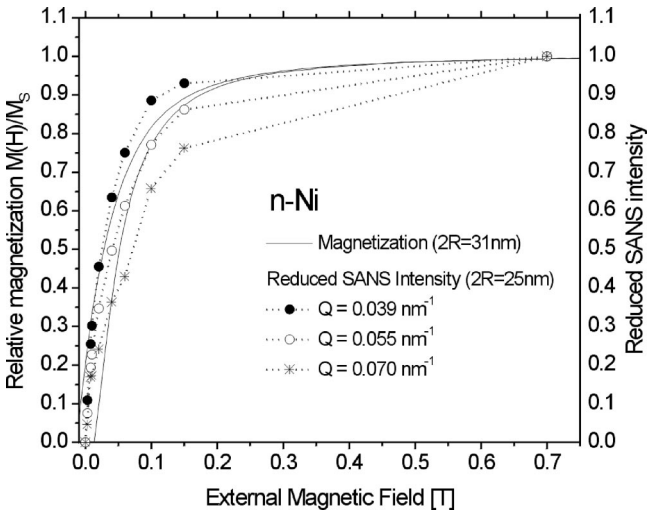

FIG. 9. Field dependence of the reduced SANS intensity (see text) measured at several Q values for a n-Ni sample with average grain size 25 nm compared with magnetization measurements on n-Ni sample with average grain size of 31 nm.

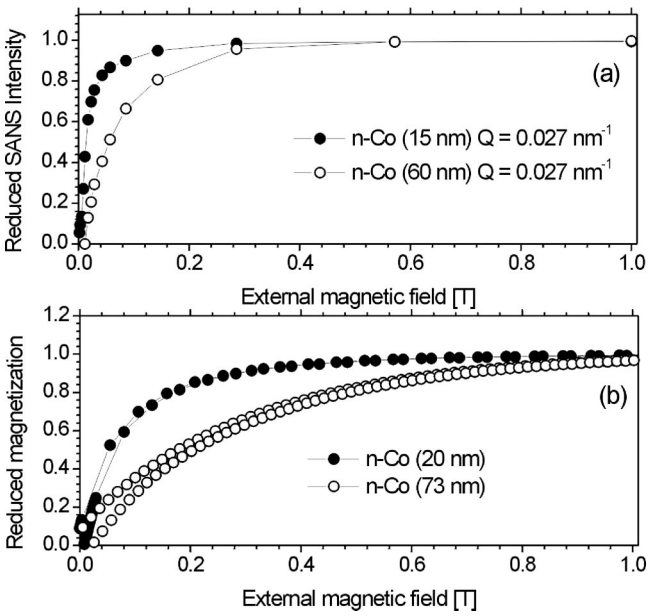

FIG. 10. (a) Field dependence of the reduced SANS intensity measured at the lowest Q value for two n-Co samples with different grain sizes of 15 and 60 nm. (b) Reduced magnetization measurements, on n-Co samples with different grain sizes of 20 and 73 nm.

e.g., 0.070 nm^{-1}. The SANS signal is sensitive to the size of the magnetic correlations, whereas the magnetization measurement gives only an average over the whole sample volume. The small Q part of the SANS signal depends predominantly on magnetic domains with large size, so we can conclude that in n-Ni the large magnetic domains tend to align along the external field direction much easier than the small ones. For the case of n-Co it was also found that the reduced SANS intensity $R(B_0,Q)$ at low Q saturates easier with the external field than at larger Q. The field dependence of $R(B_0,Q)$ observed for n-Co is not as similar to the reduced magnetization as it was found for n-Ni. The results for n-Co are shown in Fig. 10. One can see the same trend in reduced SANS intensity and reduced magnetization, i.e., for smaller grain sizes of about 20 nm both these functions saturate easier with increasing fields than for larger grain sizes of the order of 60–70 nm. This behavior is in agreement with earlier magnetization studies on n-Co (Ref. 30) where an increase of permeability with decreasing grain size was reported.

VI. CONCLUDING REMARKS

Our measurements show that in PED n-Ni and n-Co samples SANS and SAXS signals are dominated by pore scattering and reveal that the pores are distributed according to a fractal correlation function. Unfortunately we are not able to determine the grain sizes by SAS measurements because the density contrast between the grains and the grain boundaries is not large enough. It seems therefore that the PED samples are much more compact than the IGC samples and their larger density can be the reason for stronger magnetic interaction across the grain boundaries. The volume fractal geometrical properties of the pore distribution can be due to specific conditions of the pulsed electrodeposition process. The fractal correlations arising during the growth process were already reported by Witten and Sander.[44] They studied computer simulations of diffusion limited aggregation (DLA) growth of a cluster of particles and found that the density correlation function of such a cluster shows a fractal power law. The DLA model of growth was successfully applied to the interpretation of experimental studies of the growth of electrodeposited two-dimensional clusters of Cu,[45] $NiCl_2$,[46] Ag, Pb, and Zn,[47] all of which show fractal-type structures.

The observed magnetic microstructure at zero field should be compared with earlier results obtained for IGC n-Ni and n-Co. The observed domain structure was usually explained in terms of the random anisotropy model (RAM).[48] This model assumes that there is an isotropic exchange coupling between the magnetic moments in the sample due to adjacent grains having randomly oriented easy magnetization axes. When the grains are smaller than some limiting size, their local anisotropies average out and many neighboring grains become magnetically coupled which leads to the formation of domains comprising many grains. According to Ref. 48 the limiting size for such an inter-grain coupling is equal to the effective width of a Bloch wall[49]

$$\delta_w = \pi\sqrt{A/K}, \tag{11}$$

where A is the exchange constant and K is the anisotropy constant. According to the values of A and K for Ni and Co (Ref. 20) we obtain $\delta_w = 122$ nm for Ni and $\delta_w = 16$ nm for Co. The RAM predicts that for grain sizes $2R < L_{\mathrm{crit}}$ the domain sizes L_{mag} are larger than the grains and that they should scale as $L_{\mathrm{mag}} \propto R^{-3}$. For grain sizes larger than L_{crit} one should observe single domain grains. The SANS and magnetization measurements of IGC n-Fe performed by Löffler *et al.*[2–6,50] were successfully described with the use of an extended RAM model with an effective limiting size of

$L_{crit} = 35$ nm which is a value similar to the effective width of a Bloch wall in Fe, $\delta_w = 46$ nm. The same model agreed also with SANS measurements of IGC *n*-Co,[4] where for grain sizes larger than 10 nm only single grain domains were observed. The results of the present SANS studies show that the magnetic domain size for PED *n*-Ni is larger than 150 nm for all grain sizes between 15 and 70 nm in agreement with earlier SANS studies of IGC *n*-Ni.[4] Since the anisotropy of Ni is relatively small, stable single grain configurations are not expected for grain sizes below δ_w, i.e., below about 120 nm. In the case of PED *n*-Co we obtain quite different results compared to the ICG *n*-Co.[33] In our case the SANS curves does not show any saturation at low *Q*, so we can conclude that for all grain sizes ranging from 15 to 60 nm the magnetic domains are larger than 150 nm. This result is completely different from the earlier SANS studies of IGC *n*-Co (Ref. 4) which show that for grain sizes larger than 10 nm the domain size is equal to the grain size. A possible explanation of such large domains in PED *n*-Co is that due to the relatively high density of the grain boundary regions the magnetic interactions between the grains may be stronger than in IGC *n*-Co.

ACKNOWLEDGMENTS

We acknowledge financial support by the DFG in the framework of SFB 277. One of us (R.P.) is indebted to the DFG for support in the framework of GRK 232. We thank Professor R. Birringer and Dr. C. Krill for providing access to the magnetometer. We thank F. Dalla Torre for help with the density measurements and Dr. Ch. Beck for help with the SANS measurements. Thanks for the chemical analyses are due to M. Michulitz from ZCH, FZ Jülich.

*Present address: Department of Physics, University of Wales, Aberystwyth SY23 3BZ, Wales, UK.

†Corresponding author.

[1] *Nanomaterials*, edited by A. S. Edelstein and R. C. Cammarata (Institute of Physics Publishing, Bristol, 1996).

[2] W. Wagner, A. Wiedenmann, W. Petry, A. Geibel, and H. Gleiter, J. Mater. Res. **6**, 2305 (1991).

[3] J. F. Löffler, W. Wagner, H. van Swygenhoven, and A. Wiedenmann, Nanostruct. Mater. **9**, 331 (1997).

[4] J. F. Löffler, Ph.D. thesis, ETH Zürich, 1998.

[5] J. F. Löffler, J. P. Meier, B. Doudin, J.-Ph. Ansermet, and W. Wagner, Phys. Rev. B **57**, 2915 (1998).

[6] J. F. Löffler, W. Wagner, and G. Kostorz, J. Appl. Crystallogr. **33**, 451 (2000).

[7] H. Gleiter, Prog. Mater. Sci. **33**, 223 (1989).

[8] R. Birringer, H. Gleiter, H.-P. Klein, and P. Marquardt, Phys. Lett. **102A**, 365 (1984).

[9] G. Kostorz, in *Neutron Scattering, Treatise on Materials Science and Technology*, edited by G. Kostorz (Academic, New York, 1979), Vol. 19, p. 227.

[10] O. Glatter and O. Kratky, *Small Angle X-ray Scattering* (Academic Press, London, 1982).

[11] G. Bacon, *Neutron Diffraction* (Oxford University Press, Oxford, 1975).

[12] H. Natter, M. Schmelzer, and R. Hempelmann, J. Mater. Res. **13**, 1186 (1998).

[13] H. Natter, M. Schmelzer, M.-S. Löffler, A. Fitch, C. E. Krill, and R. Hempelmann, J. Phys. Chem. B **104**, 2467 (2000).

[14] I. Swanson and R. Tatge, Natl. Bur. Stand. Circ. (U.S.) **539** (1), 13 (1953); (unpublished).

[15] B. E. Warren, *X-ray Diffraction* (Addison-Wesley, Reading, 1968).

[16] C. G. Granqvist and R. A. Buhrman, J. Appl. Phys. **47**, 2200 (1976).

[17] A. Hofer and J. Peebles, J. Am. Chem. Soc. **69**, 897 (1947).

[18] J. Wagner, W. Härtl, and R. Hempelmann, Langmuir **16**, 4080 (2000).

[19] V. F. Sears, Neutron News **3**, 26 (1992).

[20] M. B. Stearns, in *Landolt-Börnstein, Numerical Data and Functional Relationships in Science and Technology III* (Springer, Berlin, 1986), Vol. 19a, p. 36.

[21] P. Strunz, J. Šaroun, A. Wiedenmann, U. Keiderling, and R. Przeniosło, J. Appl. Crystallogr. **33**, 829 (2000).

[22] B. Mandelbrot, *The Fractal Geometry of Nature* (Freeman, New York, 1982).

[23] S. K. Sinha, in *Methods in the Physics of Porous Media*, edited by P. Z. Wong (Academic Press, New York, 1999), p. 223.

[24] H. D. Bale and P. W. Schmidt, Phys. Rev. Lett. **53**, 596 (1984).

[25] P. Z. Wong, J. Howard, and Jar-Shyong Lin, Phys. Rev. Lett. **57**, 637 (1986).

[26] D. W. Schaefer, J. E. Martin, P. Witzius, and D. S. Cannell, Phys. Rev. Lett. **52**, 2371 (1984).

[27] T. Freltoft, J. K. Kjems, and S. K. Sinha, Phys. Rev. B **33**, 269 (1986).

[28] J. Weissmüller, J. Löffler, and M. Kleber, Nanostruct. Mater. **6**, 105 (1995).

[29] M. Veith, S. Faber, R. Hempelmann, S. Janssen, J. Prewo, and H. Eckerlebe, J. Mater. Sci. **31**, 2009 (1996).

[30] M. Schmelzer, Ph.D. thesis, University of Saarbrücken, 1999.

[31] U. Keiderling, *SANS Data Reduction Manual* (Hahn-Meitner Institute, Berlin, 1998).

[32] E. Jorra, H. Franz, J. Peisl, G. Wallner, W. Petry, R. Birringer, H. Gleiter, and T. Haubold, Philos. Mag. B **60**, 159 (1989).

[33] W. Wagner, H. van Swygenhoven, H. J. Höffler, and A. Wiedenmann, Nanostruct. Mater. **6**, 929 (1995).

[34] A. Michels, J. Weissmüller, A. Wiedenmann, and J. G. Barker, J. Appl. Phys. **87**, 1 (2000).

[35] J. Weissmüller, R. D. McMichael, A. Michels, and R. D. Shull, J. Res. Natl. Inst. Stand. Technol. **104**, 261 (1999).

[36] P. W. Schmidt, J. Appl. Crystallogr. **24**, 414 (1991).

[37] O. Hartmann, R. Wäppling, M. Ekström, B. Heisel, M. Schmelzer, H. Natter, and R. Hempelmann, Nanostruct. Mater. **12**, 943 (1999).

[38] St. Lauer, Z. Guan, H. Wolf, H. Natter, M. Schmelzer, R. Hempelmann, and Th. Wichert, Nanostruct. Mater. **12**, 955 (1999).

[39] H. Kisker, T. Geesmann, T. Würschum, H. Kronmüller, and H. E. Schaefer, Nanostruct. Mater. **6**, 925 (1995).

[40] L. Daroczi, D. L. Beke, G. Posgay, and M. Kis-Varga, Nanostruct. Mater. **6**, 981 (1995).

[41] M. J. Aus, B. Szpunar, A. M. El-Sherik, U. Erb, G. Palumbo, and K. T. Aust, Scr. Metall. Mater. **27**, 1639 (1992).
[42] M. Liebs, K. Hummler, and M. Fähnle, Phys. Rev. B **51**, 8664 (1995).
[43] W. Wagner, J. F. Löffler, and J. Kohlbrecher, BENSC Exp. Rep. 1995, HMI, **B536**, 232 (1996).
[44] T. A. Witten and L. M. Sander, Phys. Rev. Lett. **47**, 1400 (1981).
[45] A. S. Paranjpe, S. Bhakay-Tamhane, and M. B. Vasan, Phys. Lett. A **140**, 193 (1989).
[46] J. Z. Zhang, C. H. Zhang, and H. D. Li, J. Phys.: Condens. Matter **4**, L245 (1992).
[47] I. Mogi, M. Kamiko, and S. Okubo, Physica B **211**, 319 (1995).
[48] R. Alben, J. J. Becker, and M. C. Chi, J. Appl. Phys. **49**, 1653 (1978).
[49] B. A. Lilley, Philos. Mag. **41**, 792 (1950).
[50] J. F. Löffler, H. B. Braun, and W. Wagner, J. Appl. Phys. **85**, 5187 (1999).